Taylor & Francis
Taylor & Francis Group

Remote Sensing Letters

ISSN: 2150-704X (Print) 2150-7058 (Online) Journal homepage: http://www.tandfonline.com/loi/trsl20

Assessment of SAR speckle filters in the context of object-based image analysis

N. S. Morandeira, R. Grimson & P. Kandus

To cite this article: N. S. Morandeira, R. Grimson & P. Kandus (2016) Assessment of SAR speckle filters in the context of object-based image analysis, Remote Sensing Letters, 7:2, 150-159, DOI: 10.1080/2150704X.2015.1117153

To link to this article: http://dx.doi.org/10.1080/2150704X.2015.1117153

REMOTE SENSING LETTERS, 2016
VOL. 7, NO. 2, 150–159
http://dx.doi.org/10.1080/2150704X.2015.1117153

Taylor & Francis
Taylor & Francis Group

Assessment of SAR speckle filters in the context of object-based image analysis

N. S. Morandeira [a,b], R. Grimson[b,c] and P. Kandus[a]

[a]Instituto de Investigación e Ingeniería Ambiental, Universidad Nacional de San Martín, San Martín, Argentina; [b]Consejo Nacional de Investigaciones Científicas (CONICET), San Martín, Argentina; [c]Escuela de Ciencia y Tecnología, Universidad Nacional de San Martín, San Martín, Argentina

ABSTRACT

The initial step in most object-based classification methodologies is the application of a segmentation algorithm to define objects. In the context of synthetic aperture radar (SAR) image analysis, the presence of speckle noise might hamper the segmentation quality. The aim of this study is to assess the segmentation performance of SAR images when no filter or different filters are applied before segmentation. In particular, the performance of the mean-shift segmentation algorithm combined with different adaptive and non-adaptive filters is assessed based on both synthetic and natural SAR images. Studied filters include the non-adaptive Boxcar filter and four adaptive filters: the well-known Refined Lee filter and three recently proposed non-local filters differing, in particular, in their dissimilarity criteria: the Hellinger and the Kullback–Leibler filters are based on stochastic distances, whereas the NL-SAR filter is based on the generalized likelihood ratio. Two measures were used for quality assessment: ρ-index and κ-index. Over-segmentation was assessed by the ρ-index, the ratio of the resulting number of segments to the number of connected components of the ground-truth classes. The accuracy of the best possible classification given on the segmentation result was assessed with ground truth information by maximizing the κ-index. A Monte Carlo experiment conducted on synthetic images shows that the quality measures significantly differ for the applied filters. Our results indicate that the use of an adaptive filter improves the performance of the segmentation. In particular, the combination of the mean-shift segmentation algorithm with the NL-SAR filter gives the best results and the resulting process is less sensitive to variations in the mean-shift operational parameters than when applying other filters or no filter. The results obtained may help improve the reliability of land-cover classification analyses based on an object-based approach on SAR data.

ARTICLE HISTORY
Received 11 August 2015
Accepted 26 October 2015

1. Introduction

Most quantitative analyses in image classification have followed a per-pixel approach based on a multidimensional feature space. Nevertheless, due to the increasing use of airborne digital data and radar data the need for context-based algorithms and object-oriented image processing is increasing. Object-based image analysis (OBIA) is accurate for

CONTACT R. Grimson rgrimson@unsam.edu.ar

classifying discrete objects larger than pixel resolution, allowing multi-scale analyses and the linkage of image objects with geographical features (Blaschke et al. 2014). OBIA involves image segmentation into homogeneous objects as a fundamental step. In the context of synthetic aperture radar (SAR) image analysis, speckle noise reinforces the choice of an OBIA approach since single pixel values are not truly related to backscattering values (Lee and Pottier 2009). However, there are different strategies applied in the literature regarding the prefiltering of SAR images speckle noise: some authors filter the image before its segmentation (Evans and Costa 2013; Demers et al. 2015; Jarabo-Amores et al. 2011; Senthilnath et al. 2013) while others apply the segmentation to the noisy image directly (Campo-Becerra, Yañez-Vargas, and López-Ruíz 2014; Silva, Costa, and Melack 2010). The aim of this study is to assess the segmentation performance when no filter or different filters are applied before segmentation. In particular, we compare the performances of the mean-shift segmentation algorithm (Comaniciu and Meer 2002) when it is applied to speckled and prefiltered images. We evaluate three recently proposed non-local filters: Hellinger (Torres et al. 2014), Kullback–Leibler (Grimson, Morandeira, and Frery 2015) and NL-SAR filters (Deledalle et al. 2015), comparing them with the well-established Refined Lee filter and with the non-adaptive Boxcar filter. To complete the study, we also evaluate the segmentation quality when no filter is applied to the noisy image.

2. Materials and methods

The intensity SAR images have a particular noise, called speckle. This noise is multiplicative and follows a Gamma distribution. The presence of speckle noise might hamper the segmentation quality. To assess the contribution of prefiltering to SAR image segmentation, the combination of each proposed filter with the mean-shift segmentation algorithm is applied on both synthetic and natural SAR images. The results are interpreted using two objective quality measures. We also evaluate, for the different combinations, their stability with respect to input image data and to the mean-shift operational parameters. Next, we introduce the filters, the segmentation method, the natural and synthetic images, and the quality measures used for the quality assessment.

2.1. *Filters*

We include in the assessment three recently proposed non-local filters for speckle noise: Hellinger (Torres et al. 2014), Kullback–Leibler (Grimson, Morandeira, and Frery 2015) and NL-SAR filters (Deledalle et al. 2015). Historically the first non-local filter, NL-means, was proposed by Buades, Coll, and Morel (2005). It was based on a non-local weighted averaging of all pixels in the image and was designed to filter additive Gaussian noise. The three proposed non-local filters apply these ideas to the speckle noise. Inter alia, the three non-local filters differ in their dissimilarity criteria: the first two are based on stochastic distances whereas the NL-SAR filter is based on the generalized likelihood ratio. Moreover, the NL-SAR filter has a greater adaptivity in the sense that it automatically adapts all its parameters to the scale of local structures. This leads to a higher computational complexity of the filter that is compensated by a highly efficient parallel implementation.

The Refined Lee filter is widely used in SAR image processing since it bears an efficient noise reduction with a good conservation of the image sharpness. Hence, it is

included in the assessment as a quality reference. The non-adaptive Boxcar filter, on the other hand, indiscriminately averages neighbouring pixels in the image and is known to damage the local structures, blurring the discontinuities in the image. We include it in the analysis to assess the impact of a poor filter into image segmentation.

2.2. *Segmentation method*

Image segmentation is the process of partitioning an image into spatially continuous, disjoint and homogeneous regions (Blaschke et al. 2014), ideally related to objects on the ground and it is the foundation for further image analysis and interpretation in OBIA.

There are hundreds of segmentation algorithms (Dey, Zhang, and Zhong 2010). We have chosen the mean-shift method since it is a well-established segmentation procedure (Jarabo-Amores et al. 2011; Unnikrishnan, Pantofaru, and Hebert 2007; Campo-Becerra, Yañez-Vargas, and López-Ruíz 2014), it is completely unsupervised, and it has an efficient open source implementation (Inglada and Christophe 2009). The mean-shift segmentation method requires no human supervision or initialization besides the selection of the scale parameters. This fact renders the evaluation of the filters independent of subjective choices. Moreover, the Orfeo ToolBox multiplatform implementation is highly efficient and open source, which provides the ability to reproduce published results, interrogate the existing algorithm and to adapt it as required. This implementation can handle large images efficiently which is fundamental to process real satellite image in a reasonable time.

The mean-shift algorithm behind the segmentation procedure is a non-parametric technique for the analysis of a complex multimodal feature space used to delineate arbitrarily shaped clusters in it (Comaniciu and Meer 2002). Mean-shift-based segmentation method delineates arbitrarily shaped regions in the image by locating the modes in the density distribution space and by grouping all pixels associated with the same mode. The operational parameters for this algorithm are the spatial radius and the range radius that determine the spatial and radiometric resolution of the analysis. In order to make the comparisons more approachable and since the segmentation method is particularly sensitive to the radiometric resolution (Unnikrishnan, Pantofaru, and Hebert 2007), we fix the spatial radius to 10 pixels and analyse the results for range radii in the interval 0.5–3.5 dB.

2.3. *Natural images*

We selected three fragments of SAR intensity images with HH polarization and 3-looks to assess the performance of the proposed filters in combination with the selected segmentation procedure. These fragments represent meandering water courses in marshes. The first (N1, 10 April 2011) and second (N2, 16 November 2011) natural images correspond to X-Band COSMO-SkyMed images of the Paraná River floodplain near Santa Fe and Ramallo cities, respectively. The third image (N3, 4 March 2008) is a fragment of an L-Band ALOS/PALSAR-1 image of the Ajó Coastal Plain. While N1 and N2 include streams, N3 includes a tidal channel. Prior segmenting, backscattering coefficients were converted to decibels (dB).

In each image, two different classes are considered: water and no-water. The no-water class has a homogeneous vegetation type in each image. The polygons representing the ground truth of these classes were drawn based on closely dated high-resolution optical images from Google Earth and are shown in Figure 1. These two classes were chosen

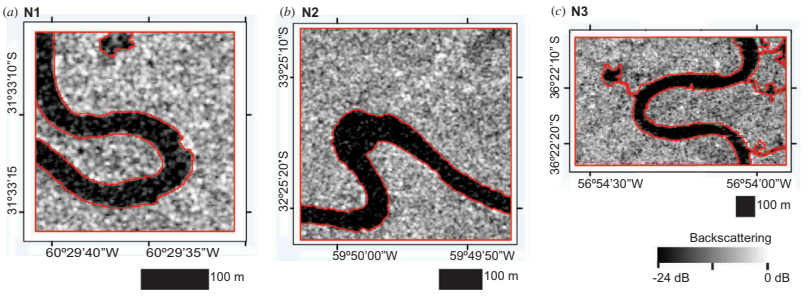

Figure 1. Three natural images (N1, N2 and N3) with the ground truth water and no-water classes delimited (see electronic version for details). Data type is single polarization (HH). N1 and N2 correspond to X-Band COSMO-SkyMed images; N3 corresponds to L-Band ALOS/PALSAR-1 images. Backscattering coefficients were converted to decibels (dB).

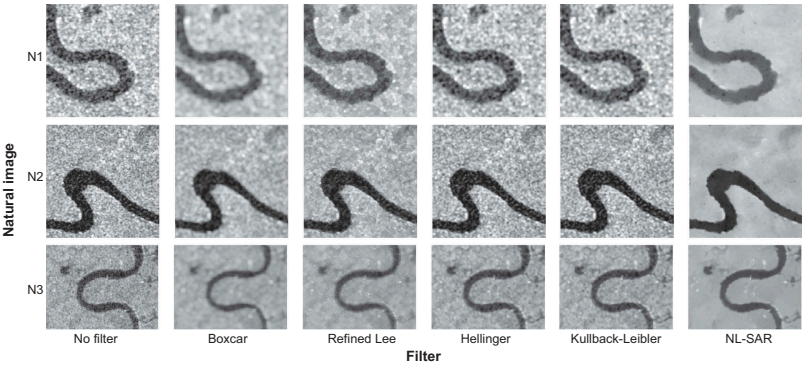

Figure 2. Original natural images (N1, N2, N3) and results of denoising each image with Boxcar, Refined Lee, Hellinger, Kullback–Leibler and NL-SAR filters. For references on the natural images, see Figure 1.

because, although knowledge of the area is required, no field work is necessary for identifying the classes. The results of the studied filters applied to these images are shown in Figure 2.

2.4. *Synthetic images*

To further analyse the proposed methods, we consider the three 127 × 127 pixel synthetic images shown in the first column of Figure 3. The first image, S1, is composed of two different kinds of regions: (i) a homogeneous background region, and (ii) homogeneous stripes and squares of different sizes. The second image, S2, is composed of five different regions plus some corner reflectors: (i) a homogeneous background region, (ii–v) four homogeneous squares with different backscattering values, and (vi) high reflectance shapes aligned in a vertical and a horizontal line simulating corner reflectors. The third image, S3, is composed of three different homogeneous regions forming a Y-shaped figure. A 3-looks speckled version of these images is shown in the second column of Figure 3 and the ones denoised with the different filters are shown in the remaining columns of the figure. Since the speckled images are created from noise-free synthetic images, we have an exact *ground truth* to assess the different classification results.

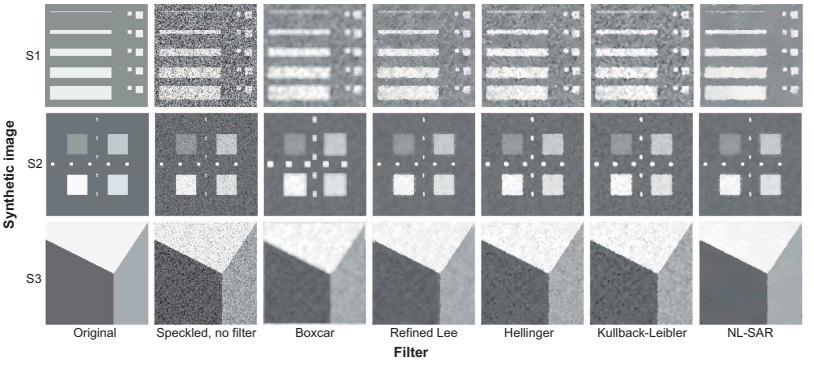

Figure 3. Original synthetic images (S1, S2, S3), speckled images with 3-looks, and result of denoising each image with Boxcar, Refined Lee, Hellinger, Kullback–Leibler and NL-SAR filters. For each synthetic image, only one randomly selected result of the 100 Monte Carlo iterations is shown. Note that the minimum number of segments is 21 for S1, 20 for S2 and 3 for S3.

2.5. *Quality measures*

Two types of error typically coexist in image segmentation: over-segmentation and under-segmentation (Liu and Xia 2010; Möller, Lymburner, and Volk 2007). Over-segmentation occurs when one semantic object is partitioned into multiple objects and leads to segments that do not represent real objects on Earth surface but fractions of these objects. The assembly of these segments into classes is then left to a classification algorithm, overloading its original task, increasing the overall computational time and eventually leading to classification errors. On the other hand, under-segmentation occurs when different semantic objects are grouped into one large image object. In this case, image segments cover more than one class. Under-segmentation introduces classification errors since all pixels in a mixed segment are assigned to a same class.

In addition to visual inspection, two quality measures that evaluate the over- and under-segmentation errors were used to assess the segmentation quality of the combination of each filter with the mean-shift segmentation algorithm. The first quality measure is related to the number of segments obtained after segmentation. Since the segments are connected sets, in order to obtain a correct classification the resulting number of segments has to be at least equal to the number of connected components of the desired classes. To allow comparisons between segmentations of different images, we define our first quality measure, the ρ-index, as the ratio of the resulting number of segments to the number of connected components of the ground-truth classes. In this way, a ρ-index greater than 1 indicates over-segmentation.

After segmentation, the segments are assigned to classes. The second quality measure is the pixel-wise classification accuracy estimated by the κ-index (Cohen 1960) between the resulting classification and the ground truth. To avoid the introduction of a particular classification algorithm that might bias the result and hamper the assessment of the segmentation procedure, we choose to assign segments to classes by maximizing the κ-index. In this way, the κ-index measures the goodness of fit of the best possible classification based on the given segmentation result and is an indicator of the under-segmentation error. It does not assume equal cardinality of object sizes or

between the number of segments and ground-truth classes and allows comparisons between segmentations of different images and segmentations of the same image.

The three natural images considered (Figure 1) have only two classes and four, three and six connected components, respectively. In the synthetic images (Figure 3) there are two, six and three different classes, and 21, 20 and 3 connected components, respectively. For the assessment of the synthetic images we employed a Monte Carlo method, repeating the complete process – speckle the noise-free image, filter (or not) the noisy image, segment the filtered image, classify the segments, assess the result – 100 times independently for each synthetic image.

3. Results

3.1. *Natural images*

Quality measures for the results of the different experiments for the natural images are shown in Figure 4. The plot shows that the number of segments decreases as the range radius (h_r) increases, whereas the trend for the κ-index depends on the image. For the first image, N1, over-segmentation is observed for h_r values lower than 1.5. Also, for h_r higher than 2 the κ-index is relatively low. The only exception for both patterns is the NL-SAR filter that leads to a maximum of 15 segments and a κ-index higher than 93% for every value of h_r in the studied range. When no filter is applied the results are of a poor quality for every parameter considered.

For the second image, N2, the κ-index is always higher than 93% and it increases with the range radius for all experiments but the Boxcar filter. For low values of h_r all the experiments but the one involving the NL-SAR filter over-segment the image.

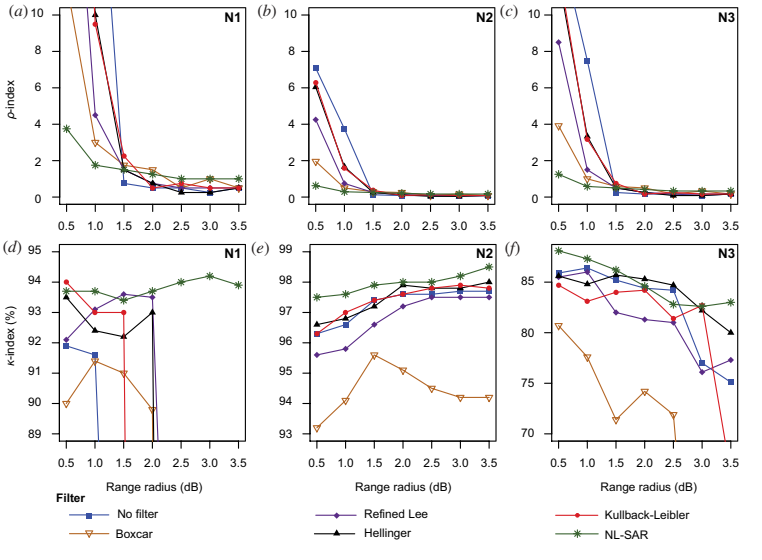

Figure 4. Quality measures for the natural images N1, N2 and N3. The mean-shift algorithm was used to segment the images, with spatial radius set to 10 pixels and range radius ranging between 0.5 and 3.5. For details on the quality measures (ρ-index and κ-index), see the text. To improve the reading, the scale varies in sub-figures (*d*), (*e*) and (*f*).

For the third image, N3, both the number of segments and the κ-index decrease with the range radius. The NL-SAR filter is the most robust also in this case, in the sense that both the increase in the number of segments and the decrease of the κ-index are moderate. Good results are obtained in this image for the Hellinger filter and for the segmentation on the original image with no filter applied.

3.2. *Synthetic images*

Quality measures obtained for each different synthetic-image experiment are summarized in Figure 5. The plotted values represent the average of the 100 replications of each Monte Carlo experiment.

When no filter is applied an important over-segmentation takes place for the three selected phantoms (see Figure 5). When filtering, the number of segments obtained remains bounded and decreases with the range radius. In all the experiments, the κ-index decreases as h_r increases. For the three synthetic images, the κ-index is higher when an adaptive filter is applied before segmentation. The NL-SAR filter performs better than the remaining combinations, while the Hellinger filter is generally in the second place.

In the first image, S1, κ-indices higher than 80% are obtained with h_r values lower than 2.5 for all filters but for the Boxcar and no-filter. The adaptive filters yield better results, being NL-SAR slightly better than the others. For the second image, S2, NL-SAR also has a superior performance, while the Refined Lee filter performs slightly better than Hellinger filter, and the Kullback–Leibler filter occupies the last place among the adaptive filters. Lastly, the third image, S3, also shows a higher performance of the NL-SAR filter, followed by the Refined Lee filter and, next, by the Hellinger and Kullback–Leibler filters.

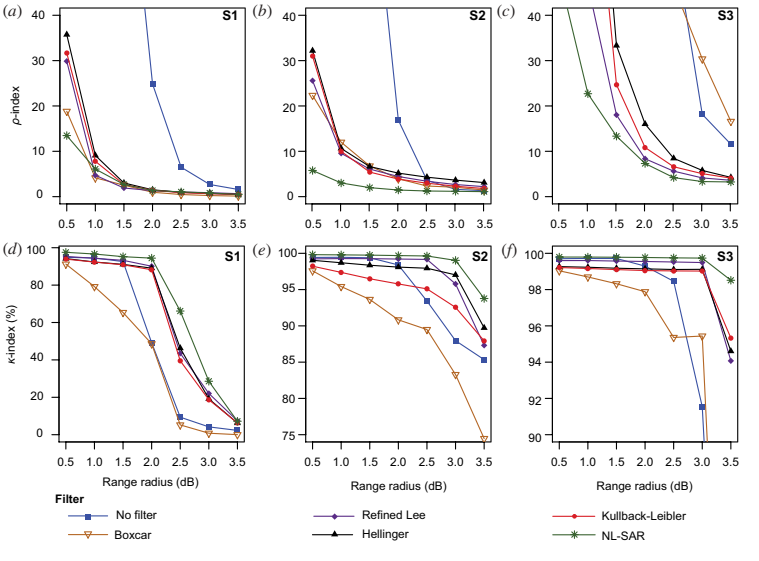

Figure 5. Quality measures for the synthetic images: S1, S2 and S3. The mean values of the quality measures for the 100 iterations of the Monte Carlo experiment are shown. The mean-shift algorithm was used to segment the images, with spatial radius set to 10 pixels and range radius ranging between 0.5 and 3.5. For details on the quality measures (ρ-index and κ-index), see the text. To improve the reading, the scale varies in sub-figures (*d*), (*e*) and (*f*).

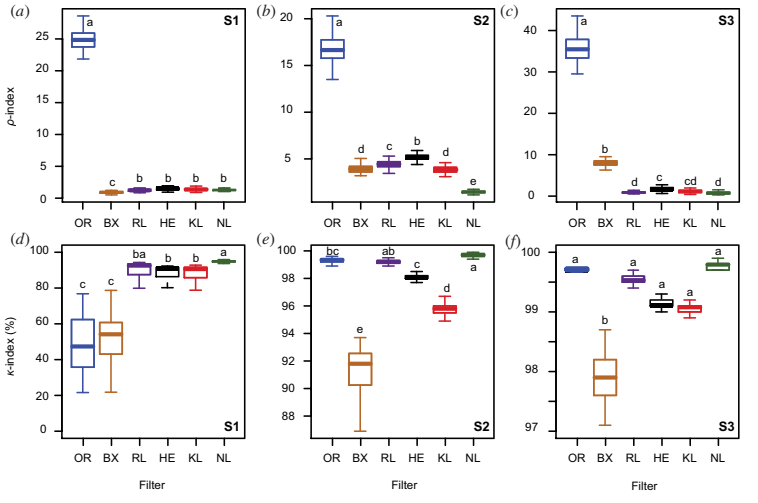

Figure 6. Quality measures for the synthetic images: S1, S2 and S3; for $h_r = 2$ dB. A total of 100 Monte Carlo iterations were computed for each filter. The letters represent significant differences in the quality measures between the filters (ANOVA tests, followed by Tukey comparisons), at 0.01 significance level. To improve the reading, the scale varies between sub-figures.

Since in all the cases the best results are obtained for intermediate range radius (due to the trade-off between the number of segments and the κ-index), we fix $h_r = 2$ to construct a box plot showing the summary of the results of the 100 iterations of the Monte Carlo experiment (Figure 6). An analysis of variance (ANOVA, $p<0.01$) of these results reveals that the number of segments is significantly higher for the original image than for the filtered images. The filter yielding the lowest number of segments depends on the synthetic image: Boxcar filter for S1; NL-SAR for S2; and NL-SAR, Kullback–Leibler and Refined Lee for S3. Regarding the κ-index, the Boxcar filter always leads to low values, as well as the original image for S1. NL-SAR filter always leads to high κ-index values, as well as the Refined Lee filter ($p<0.01$).

4. Conclusion

In this paper, the mean-shift segmentation algorithm has been applied to six images, both pure and filtered with each proposed filters, and the results assessed in terms of two quality measures that evaluate the over- and under-segmentation errors. Segmenting SAR data and classifying objects instead of pixels may be helpful to deal with the speckle noise. However, we have shown that applying an accurate speckle filter is preferable to improve the segmentation performance. The results based on both natural and synthetic images indicate that the use of an adaptive filter before segmentation improves the segmentation quality.

The combination of the mean-shift segmentation algorithm with the NL-SAR filter gives the best results, with low ρ-indexes and high κ-indexes. Also, a segmentation performed after NL-SAR filtering results less sensitive to variations in the mean-shift operational parameters. Moreover, its performance is also more stable over different

images than the performance of the other studied filters. The Hellinger and Kullback–Leibler filters offer a good performance, comparable with the Refined Lee filter. When no filter is applied before segmentation, an extreme over-segmentation is observed due to the speckle noise. The assembly of these segments into classes is then left to a classification algorithm, overloading its intended task, increasing the overall computational time and eventually leading to classification errors. However, it becomes clear that not filtering is better than the application of the Boxcar filter that blurs the image and prevents a reasonable delineation of the ground-truth classes.

We do not claim that our results have any implication about the quality of the studied filters as speckle filters. They are evaluated in the context of a specific task and for a particular segmentation algorithm. However, it becomes clear that the use of the NL-SAR filter gives the best results in this context, yielding more accurate classifications, and being more robust. The results obtained may help to improve the reliability of land-cover classification analyses based on image objects obtained by segmenting SAR data. Based on the results obtained for the three studied natural images, we suggest that our conclusions may be extended to other floodplain and coastal wetlands. Moreover, the results obtained for the synthetic images suggest that the use of the NL-SAR filter may improve the segmentation results on general SAR images.

Acknowledgements

Cosmo-SkyMed imagery was acquired through a project with Agenzia Spaziale Italiana and ALOS/PALSAR-1 imagery through an agreement with Comisión Nacional de Actividades Espaciales (CONAE, Argentina). We thank Laura San Martín for her help in ground truth mapping and Alejandro Frery for his valuable comments on a previous version of this manuscript.

Disclosure statement

No potential conflict of interest was reported by the authors.

Funding

This work was funded by the ANPCyT [PICTO-CIN 22, PICT 2012-2403 and PICT 2014-0824].

ORCID

N. S. Morandeira http://orcid.org/0000-0003-3674-2981

References

Blaschke, T., G. J. Hay, M. Kelly, S. Lang, P. Hofmann, E. Addink, R. Q. Feitosa, et al.. 2014. "Geographic Object-Based Image Analysis: Towards a New Paradigm." *ISPRS Journal of Photogrammetry and Remote Sensing* 87: 180–191. doi:10.1016/j.isprsjprs.2013.09.014.

Buades, A., B. Coll, and J.-M. Morel. 2005. "A Non-Local Algorithm for Image Denoising." In *Conference on Computer Vision and Pattern Recognition, IEEE Computer Society. CVPR 2005*. vols 2, 60–65. Piscataway, NJ: IEEE. doi:10.1109/CVPR.2005.38.

Campo-Becerra, G. D., J. I. Yañez-Vargas, and J. A. López-Ruì. 2014. "Texture Analysis of Mean Shift Segmented Low-Resolution Speckle-Corrupted Fractional SAR Imagery through Neural Network Classification." In *Progress in Pattern Recognition, Image Analysis, Computer Vision, and Applications*, 998–1005. Basel: Springer.

Cohen, J. 1960. "A Coefficient of Agreement for Nominal Scales." *Educational and Psychological Measurement* 20 (1): 37–46. doi:10.1177/001316446002000104.

Comaniciu, D., and P. Meer. 2002. "Mean Shift: A Robust Approach toward Feature Space Analysis." *IEEE Transactions on Pattern Analysis and Machine Intelligence* 24 (5): 603–619. doi:10.1109/34.1000236.

Deledalle, C.-A., L. Denis, F. Tupin, A. Reigber, and M. Jäger. 2015. "NL-SAR: A Unified Nonlocal Framework for Resolution-Preserving (Pol)(In)SAR Denoising." *IEEE Transactions on Geoscience and Remote Sensing* 53 (4): 2021–2038. doi:10.1109/TGRS.2014.2352555.

Demers, A.-M., S. N. Banks, J. Pasher, J. Duffe, and S. Laforest. 2015. "A Comparative Analysis of Object-Based and Pixel-Based Classification of RADARSAT-2 C–Band and Optical Satellite Data for Mapping Shoreline Types in the Canadian Arctic." *Canadian Journal of Remote Sensing* 41 (1): 1–19. doi:10.1080/07038992.2015.1020361.

Dey, V., Y. Zhang, and M. Zhong. 2010. "A Review on Image Segmentation Techniques with Remote Sensing Perspective." In *ISPRS TC VII Symposium - 100 Years ISPRS*, eds. W. Wagner, and B. Székely. Vol. XXXVIII. *Vienna, Austria*: IAPRS.

Evans, T. L., and M. Costa. 2013. "Landcover Classification of the Lower Nhecolândia Subregion of the Brazilian Pantanal Wetlands Using ALOS/PALSAR, RADARSAT-2 and ENVISAT/ASAR Imagery." *Remote Sensing of Environment* 128: 118–137. doi:10.1016/j.rse.2012.09.022.

Grimson, R., N. S. Morandeira, and A. Frery. 2015, July. "Comparison of Nonlocal Means Despeckling based on Stochastic Measures." *Geoscience and Remote Sensing Symposium, 2015 IEEE International, IGARSS 2015*. vols 103091–3094. Milan, Italy. Piscataway, NJ: IEEE. doi:10.1109/IGARSS.2015.7326470.

Inglada, J., and E. Christophe. 2009. "The Orfeo Toolbox Remote Sensing Image Processing Software." In *Geoscience and Remote Sensing Symposium, 2009 IEEE International, IGARSS 2009*. vols 4, 733–736. Piscataway, NJ: IEEE. doi:10.1109/IGARSS.2009.5417481.

Jarabo-Amores, P., M. Rosa-Zurera, D. De La Mata-Moya, R. Vicen-Bueno, and S. Maldonado-Bascon. 2011. "Spatial-Range Mean-Shift Filtering and Segmentation Applied to SAR Images." *IEEE Transactions on Instrumentation and Measurement* 60 (2): 584–597. doi:10.1109/TIM.2010.2052478.

Lee, J. S., and E. Pottier. 2009. *Polarimetric Radar Imaging: From Basics to Applications*. Boca Raton, FL: CRC Press.

Liu, D., and F. Xia. 2010. "Assessing Object-Based Classification: Advantages and Limitations." *Remote Sensing Letters* 1 (4): 187–194. doi:10.1080/01431161003743173.

Möller, M., L. Lymburner, and M. Volk. 2007. "The Comparison Index: A Tool for Assessing the Accuracy of Image Segmentation." *International Journal of Applied Earth Observation and Geoinformation* 9 (3): 311–321. doi:10.1016/j.jag.2006.10.002.

Senthilnath, J., H. V. Shenoy, R. Rajendra, S. N. Omkar, V. Mani, and P. G. Diwakar. 2013. "Integration of Speckle De-Noising and Image Segmentation Using Synthetic Aperture Radar Image for Flood Extent Extraction." *Journal of Earth System Science* 122 (3): 559–572. doi:10.1007/s12040-013-0305-z.

Silva, T. S. F., M. Costa, and J. M. Melack. 2010. "Spatial and Temporal Variability of Macrophyte Cover and Productivity in the Eastern Amazon Floodplain: A Remote Sensing Approach." *Remote Sensing of Environment* 114 (9): 1998–2010. doi:10.1016/j.rse.2010.04.007.

Torres, L., S. J. S. Sant'Anna, C. Da Costa Freitas, and A. C. Frery. 2014. "Speckle Reduction in Polarimetric SAR Imagery with Stochastic Distances and Nonlocal Means." *Pattern Recognition* 47 (1): 141–157. doi:10.1016/j.patcog.2013.04.001.

Unnikrishnan, R., C. Pantofaru, and M. Hebert. 2007. 'Toward Objective Evaluation of Image Segmentation Algorithms.' *IEEE Transactions on Pattern Analysis and Machine Intelligence* 29 (6): 929–944. doi:10.1109/TPAMI.2007.1046.